



# Probing the intracellular organic matters released from the photocatalytic inactivation of bacteria using fractionation procedure and excitation-emission-matrix fluorescence



Guocheng Huang<sup>a</sup>, Tsz Wai Ng<sup>a</sup>, Taicheng An<sup>b, \*\*</sup>, Guiying Li<sup>b</sup>, Dehua Xia<sup>a</sup>, Ho Yin Yip<sup>a</sup>, Huijun Zhao<sup>c</sup>, Po Keung Wong<sup>a, \*</sup>

<sup>a</sup> School of Life Sciences, The Chinese University of Hong Kong, Shatin, NT, Hong Kong, China

<sup>b</sup> Institute of Environmental Health and Pollution Control, School of Environmental Science and Engineering, Guangdong University of Technology, Guangzhou 510006, China

<sup>c</sup> Centre for Clean Environment and Energy, Griffith Scholl of Environment, Griffith University, Queensland 4222, Australia

## ARTICLE INFO

### Article history:

Received 8 September 2016

Received in revised form

19 December 2016

Accepted 19 December 2016

Available online 21 December 2016

### Keywords:

Photocatalysis

*Escherichia coli*

Intracellular organic matters

Fractionation procedure

3-D fluorescence

## ABSTRACT

Photocatalysis provides a “green” and effective strategy for water disinfection. During the photocatalytic disinfection process, intracellular organic matter (IOM) from bacterial cells may be released into the bulk solution. In this study, the role of released IOM in the photocatalytic bacterial inactivation was investigated by fractionation procedure and fluorescence excitation-emission-matrix (EEM) combined with parallel factor analysis (PARAFAC) approaches. The normal bacterial cells treated by TiO<sub>2</sub>-UVA in the presence and absence with fractionated IOM results implied that the released IOM would be either absorbed on the surface of the photocatalysts or reacted by the photo-generated reactive species, and thereby affecting the kinetics of photocatalytic bacterial inactivation. Fluorescence EEM-PARAFAC results showed that two components (C1 and C3) associated with tryptophan- and tyrosine-like proteins were released. While another two components (C2 and C4) were the oxidation products, and their intensities were found to negatively correlate with those of C1 and C3, respectively. Microtox<sup>®</sup> test results indicated that toxicity occurred during the photocatalytic bacterial inactivation process. The toxicity was found to decrease after the bacteria were completely inactivated, and completely removed if provided a sufficient reaction time. Of particular interest is that a significant high linear correlation was observed between the toxicity and the maximum fluorescence intensity of C4. The results and information obtained in this study will be important for further developing photocatalysis in water/wastewater disinfection.

© 2016 Elsevier Ltd. All rights reserved.

## 1. Introduction

Photocatalysis has emerged as a promising disinfection alternative for chlorination in water/wastewater treatment (Shannon et al., 2008). Unfortunately, the mechanisms and kinetics of photocatalytic bacterial inactivation have not been fully understood. Well accepted mechanism is that the photo-generated reactive oxygen species (ROSs) attack the cell membrane, followed by the release of intracellular organic matters (IOM) and their oxidation, and eventually leading to cell inactivation (Maness et al., 1999;

Carre et al., 2014). In addition to the mechanism by which bacterial cells are inactivated, the released IOM and their transformation products need careful assessment and consideration, due to the fact that the quality of organic matter could be an important parameter of water.

The release of organic matters into the bulk solution from the bacterial cells during the photocatalytic inactivation was well-evidenced by many studies by showing an increase in bulk total organic carbon (TOC) content (Leung et al., 2008). However, only TOC content is not adequate enough to fully understand the characteristics of the released organic matters. Given that the microbial inactivation is typically the last process of a water/wastewater treatment plant, the characteristics of the organic matters in the resultant water after photocatalytic treatment might be of particular importance to the consumers of drinking water or the quality

\* Corresponding author.

\*\* Corresponding author.

E-mail addresses: [antc99@gig.ac.cn](mailto:antc99@gig.ac.cn) (T. An), [pkwong@cuhk.edu.hk](mailto:pkwong@cuhk.edu.hk) (P.K. Wong).

of receiving water systems (Dietrich and Burlingame, 2015). A comprehensive study of the released organic matters from bacterial cells during the photocatalytic inactivation process is needed.

The release profile of organic matters from live bacterial cells during the photocatalytic inactivation of bacteria is difficult to study because it is likely a complex process. For instance, the organic matters in the bulk could be either originated from the intracellular regions, namely intracellular organic matters (IOM), or the cell membrane. The released organic matters from inside the bacterial cells would likely influence the inactivation of the remaining cells differently compared with the cell membrane debris due to their different chemical properties. Moreover, the behavior of the released organic matters are rather dynamic; they could be either further degraded by the ROSs or adsorbed onto the surface of photocatalysts and thus making their characterization and quantification biased. Recently, Li et al. (2014) and Korak et al. (2015) developed a fractionation procedure to get in-depth knowledge of algae-derived IOM in the water treatment process such as filtration and disinfection. They fractionated the living cells into non-living IOM using physical method (e.g. freeze-thaw cycles or sonication) and subsequently subjected to *in vitro* treatment. This fractionation procedure could aid in the investigation on how IOM plays a role in the corresponding treatment and draw insight into the evolution profile of the IOM. To the best of our knowledge, no previous study has applied fractionation procedure to study the released organic matters in the photocatalytic bacterial inactivation.

The structural and compositional information on the organic matters in water have typically been obtained with bulk parameters including TOC, UV absorbance and SUVA values (Hu et al., 2003). More specific parameters such as malondialdehyde (MDA) (Maness et al., 1999), carboxylic acids (Pigeot-Remy et al., 2011, 2012), carboxylated proteins (Thabet et al., 2014) and N-nitrosodimethylamine (Wang et al., 2014) have been successfully characterized the organic matters in disinfection process, with an attempt to probe their possible relationship with disinfection kinetic and toxicity of the treated water. Nevertheless, these methods are usually suffered from relatively low detection limit, or require expensive equipment with chemical reagents and complex preparation procedures. As such, the lack of robust real-time approach to evaluate the composition and properties of the released organic matters from the bacterial cells during the photocatalytic inactivation process remains a major challenge for a precise and comprehensive understanding of this issue.

Recently, fluorescence excitation–emission–matrix (EEM) spectroscopy has received much attention on studying of environmental samples due to its effective and sensitive nature in analysis of the fluorescent organic matter fractions (fluorophores), based on their characteristic fluorescence intensities and differences in the wavelength maxima (Hudson et al., 2007; Ishii and Boyer, 2012). However, the overlap of the peaks was usually observed in EEM contour, thus making the interpretation of EEM contour invalid solely based on visual inspection approach. The parallel factor analysis (PARAFAC) is a widely used method to mathematically separate organic matters into chemically independent fluorescence components. Fluorescence EEM combined with PARAFAC has been successfully applied to probe the transformation of dissolved organic matters in environmental water samples (Baghoth et al., 2011; Meng et al., 2013; Valencia et al., 2014; Yang et al., 2014). Despite its wide usage and increasing applications, so far, EEM-PARAFAC has not been used to characterize the organic matters released from the cells during photocatalytic bacterial inactivation.

The primary objectives of this study are to evaluate the released organic matter during the photocatalytic bacterial inactivation process in order to (i) better understand how the released organic

matters have an impact on the photocatalytic bacterial inactivation mechanisms; (ii) provide in-depth information on the quality of resultant water using fractionation procedure and fluorescence EEM combined with PARAFAC factor analysis; and more importantly, and (iii) assess the toxicity of water resulted from photocatalytic bacterial inactivation.

## 2. Methods

### 2.1. Cell cultures and fractionation procedure

*Escherichia coli* (*E. coli*) K-12 was used as model bacteria and cultured according to our previous studies (Gao et al., 2012; Wang et al., 2012). In brief, fifty mL cells were cultured in 50 mL Nutrient Broth (Lab M, Lancashire, UK) solution at 37 °C for 18 h to reach stationary phase with a cell density of  $\sim 2 \times 10^9$  colony forming unit per milliliter (cfu/mL). The culture was then washed with sterilized saline (0.9% NaCl) solution twice by centrifugation at 13000 rpm for 10 min to remove metabolites prior to use.

In the fractionation procedure, the pellet was subsequently resuspended in 50 mL ultrapure water, and lysed through 30 cycles of short burst of 30 s sonication via a sonicator probe (Vibra Cell, Sonics & Materials, USA) at 50% intensity (600 W maximum), followed by intervals of 30 s for cooling. During the whole lysis process, the suspension was immersed in ice-water bath for cooling. The suspension containing the lysates was then centrifuged at 13,000 rpm for 10 min to separate different fractions. The supernatant fraction was gently filtered by a sterile 0.2  $\mu\text{m}$  syringe filter (Acrodisc 4612) and the organic matters in the filtrate were designated as IOM standard. The pellet was washed twice with ultrapure water and designated as cell debris.

### 2.2. Photocatalytic experiments

The photocatalytic inactivation experiments were conducted in a photocatalytic reactor by using a UVA lamp (emission peak at 365 nm) as light source and 100 mg/L TiO<sub>2</sub> (P25, Degussa, German) as the photocatalyst with the volume of reaction mixture of 50 mL. To investigate how the different cellular fractions affect the photocatalytic inactivation of bacteria, the as-prepared fractions of IOM or/and cell debris were externally spiked into a  $\sim 2 \times 10^7$  cfu/mL (7 log) live *E. coli* suspensions to adjust to a final equivalent cell density of  $\sim 2 \times 10^8$  cfu/mL (8 log) for photocatalytic inactivation experiments. The photocatalytic inactivation of *E. coli* cells alone in concentrations of  $\sim 2 \times 10^7$  cfu/mL and  $\sim 2 \times 10^8$  cfu/mL were also conducted as control experiments. At different time intervals, one mL aliquot was collected from each experiment and serially diluted with sterilized saline solution; 0.1 mL of the diluted sample was then immediately spread onto nutrient agar (Lab M, Lancashire, United Kingdom) plates. Subsequently, the agar plates were incubated at 37 °C for 24 h to determine the number of surviving cells (in cfu). All the above experiments were carried out in triplicates.

Besides, the absorbance and fluorescence EEM spectra evolution of IOM and cell debris treated by photocatalysis were monitored as compared to the released organic matters from photocatalytic inactivation of live *E. coli* cells. At different time intervals, three mL aliquots of the suspensions were taken from the each reaction mixture and filtered through 0.2  $\mu\text{m}$  syringe filter for analyses.

### 2.3. Chemical measurements and spectroscopic analyses

The total organic carbon (TOC) and total nitrogen (TN) of the bulk samples obtained from the photocatalytic inactivation of 8 log *E. coli* cells, as well as the filtrate in the fractionation procedure were analyzed using a TOC-TN analyzer (TOC-V, Shimadzu, Japan).

Cell debris derived from the fractionation procedure of 50 mL cells were freeze-dried and then the TOC concentration in the cell debris was measured by a TOC Analyzer (Shimadzu, Japan) combined with a solid sample combustion unit (Shimadzu, Japan). The protein concentrations were also measured according to Bradford assay (Zor and Selinger, 1996) using bovine serum albumin (BSA) as a standard.

The absorption spectra of the bulk samples were obtained by scanning the absorbance at the wavelengths from 200 to 600 nm via a UV–visible spectrophotometer (LabTech, USA) at a resolution of 1 nm.

The three-dimensional EEM spectra of the bulk samples were obtained by a fluorescence spectrometer (F-7000, Hitachi, Japan) with excitation wavelengths in the range of 200–500 nm in 5 nm intervals and with emission wavelengths in the range of 290–550 nm in 5 nm intervals. The emission and excitation slits were fixed at 10 nm, and the scanning speed was 12000 nm/min. Second-order Raleigh scattering in the EEM measurements was eliminated using a 290 nm emission cutoff filter. According to suggested protocols of the manufacturer, the instrument was corrected for excitation and emission prior to use. The fluorescence intensities of each sample were calibrated to Raman unit (R.U.) through dividing each intensity by the integrated intensities of Raman peak (371–428 nm) of ultrapure water at excitation of 350 nm (Lawaetz and Stedmon, 2009). The inner filter effect was minimized by diluting the samples to their UV absorbance at 254 nm less than  $0.2 \text{ cm}^{-1}$ . The contour plots of the EEM dataset were visualized using Matlab 7.0.

## 2.4. Statistic analysis

### 2.4.1. PARAFAC analysis

The PARAFAC analysis of the EEM datasets is based on well-established principles (Bagthoth et al., 2011). In brief, an alternating least squares algorithm is applied to minimize the sum of squared residuals in a trilinear model, thus allowing the deconvolution of the overlapped EEM spectra into independent components as depicted in the following equation:

$$X_{ijk} = \sum_{f=1}^F a_{if} b_{jf} c_{kf} + \varepsilon_{ijk} \quad i = 1, \dots, I; j = 1, \dots, J; k = 1, \dots, K; \quad (1)$$

where  $x_{ijk}$  is the fluorescence intensity of the  $i$ th sample at the  $k$ th excitation and  $j$ th emission wavelength;  $a_{if}$  is directly proportional to the concentration of the  $f$ th fluorophore in the  $i$ th sample (defined as scores),  $b_{jf}$  and  $c_{kf}$  are estimates of the emission and excitation spectra respectively for the  $f$ th fluorophore (defined as loadings),  $F$  is the number of fluorophores (components) and  $\varepsilon_{ijk}$  is the residual element, representing the unexplained variation in the model. PARAFAC analysis was performed using the DOMFlour toolbox of the Matlab software package, which can decompose the EEM spectrum into relatively independent fluorescent components and can perform residual errors and split-half diagnostics. The DOMFlour tool box and tutorial can be downloaded freely via [http://www.models.life.ku.dk/al\\_domfluor](http://www.models.life.ku.dk/al_domfluor) (Stedmon and Bro, 2008). In this study, PARAFAC modeling between two and nine components were generated. Finally, according to the residuals and split-half analysis of the PARAFAC modeling, the number of components could be determined.

### 2.4.2. Cluster analysis

In this study, the cluster analysis was applied to the EEM datasets using the minimum-distance method, as employed in the Matlab 7.0. A shorter distance between clusters indicates a greater

similarity. The data point of each EEM dataset was normalized by the sum of its dataset to qualitatively reveal the similarities of the shape of EEM regardless of the concentrations of the fluorophores in the samples. Details of the procedures can be found in Fig. S1 in Supporting Information.

Pearson's correlation analysis was carried out using SPSS 18 software (SPSS, Chicago) and calculated correlation coefficient  $R$  was used to evaluate the correlation between two parameters. Linear regression was performed by Origin 8.5.

## 2.5. Toxicity test

The Microtox<sup>®</sup> test was used to assess the total toxicity of the treated water from photocatalytic inactivation of normal *E. coli* cells at different reaction time. This test takes the reduction in bioluminescence of the marine bacterium *Vibrio fischeri* after exposure to toxic compounds as endpoints and was carried out according to instructions provided by the manufacturer using a Microtox 500 analyzer (Azur Environmental, USA) coupled with a Microtox-OmniTM software. This test was chosen because it is a simple, rapid (15 min), and reproducible acute toxicity test. For each test, the bioluminescence of *Vibrio fischeri* exposed to duplicates of 4 concentrations (29.3%, 44%, 66.0%, and 99.0% of sample) plus a blank (0% of sample) was measured. The obtained data was used to calculate the EC50, which is the median sample concentration that causes a 50% reduction in bacterial bioluminescence. Toxicity units (TU) were used to standardize results from the following equation:

$$TU = \frac{100}{EC_{50}(15 \text{ min})} \quad (2)$$

## 3. Results and discussion

### 3.1. Impact of IOM and cell debris on photocatalytic inactivation kinetics

Fig. 1a compares the photocatalytic inactivation kinetics of bacteria cells in the presence and absence of external bacterial fractions. It was observed that in the absence of external bacterial fractions, both the inactivation curves of the 7 and 8 log initial cell density exhibit similar shapes, which can be roughly divided into three stages. In the first 20 min for the 7 log and 30 min for 8 log initial cell density (Stage I), both inactivation kinetics were subjected to a log-linear decay in cell density, suggesting first order exponential decreases in cell populations. Thereafter, the reaction processes decelerated for a certain period (from 30 min to 2 h for 8 log cell density, from 20 min to 60 min for 7 log cell density) (Stage II), followed by another log-linear decay in cell density until complete inactivation (Stage III). Previously, many studies observed that a deceleration at the end of the reaction, which is known as the “tailing” (Marugan et al., 2008; Chong et al., 2010). The reason for the tailing has not yet well understood. One possibility was proposed as that variation in bacterial population that became resistant to the photocatalysis (Lambert and Johnston, 2001). In principle, the major ROS in the TiO<sub>2</sub>-UVA system is the highly active hydroxyl radical ( $\cdot\text{OH}$ ) with a relatively high redox potential of +2.8 eV (Dalrymple et al., 2010), that can virtually oxidize all forms biomolecules. Besides, we also observed completely inactivation with prolonged reaction time (Stage III). As such, the generation of ROS-resistant bacteria is not likely to occur. A different possibility was that the competition for the ROS between the remaining viable cells and the organic matters released from the lysed cell (Benabbou et al., 2007). In addition, there is also

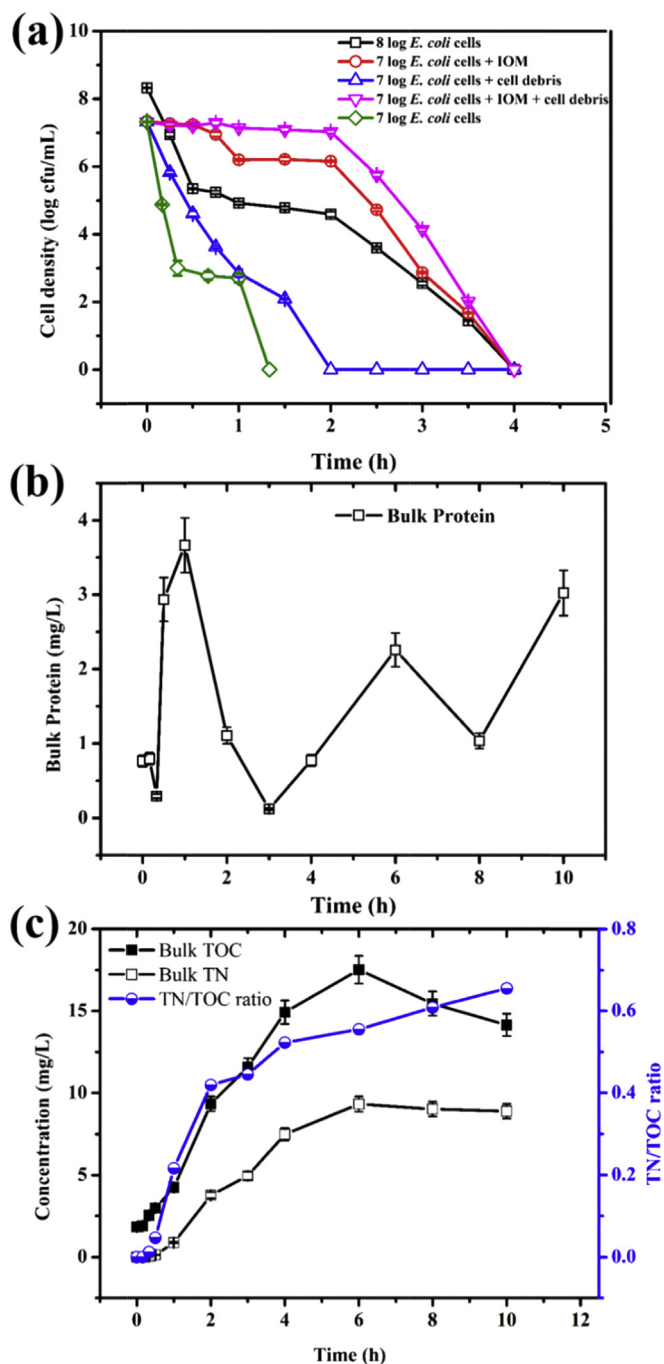


**Fig. 1.** (a) Photocatalytic inactivation kinetics of bacterial cells in the presence and absence of external spiking bacterial fractions of IOM or cell debris under  $\text{TiO}_2$ -UVA; (b) Evolution of the bulk protein concentrations and (c) bulk TOC, TN concentrations, TN/TOC ratio during the photocatalytic inactivation of 8 log *E. coli* cells under  $\text{TiO}_2$ -UVA. Bars represent the standard deviation of three replicates.

possibility that there is a competition for the photon between the photocatalysts and released organic matters (Marugan et al., 2010). Collectively, the deceleration of photocatalytic inactivation efficiency highlighted the significance of released organic matters in affecting photocatalytic bacterial inactivation process.

To investigate how different fractions of bacterial cells affect the photocatalytic inactivation, the IOM and cell debris were initially spiked into the reaction mixtures with an equivalent cell density of  $2 \times 10^8$  cfu/mL (8 log). For instance, cells of  $2 \times 10^7$  cfu/mL initial

density (7 log) were added with IOM or/and cell debris of equivalent cell density of  $1.8 \times 10^8$  cfu/mL, corresponding to a total equivalent cell density of  $2 \times 10^8$  cfu/mL. Under all conditions, the bacterial cells could be completely inactivated within 4 h, but different fractions had different effect on the photocatalytic inactivation kinetics (Fig. 1a). It can be seen that a lag or plateau in the first 30 min of the reaction, known as “shoulder”, appeared in the inactivation curves with initial addition of IOM and the inactivation efficiency was greatly reduced during all the reaction time, indicating that the presence IOM greatly inhibited the photocatalytic inactivation efficiency. In contrast, the addition of cell debris did not confer a “shoulder” in the inactivation curves, but the inactivation followed a first order decay and achieved complete inactivation within 2 h. This result suggested that the cell debris, which is mainly from the cell membrane and cell wall, play a moderate role in inhibiting the photocatalytic inactivation. This could be reasoned by the fact the cell debris are mainly composed of fatty acids, which were widely regarded to be susceptible to peroxidation (Dalrymple et al., 2010). A radical chain reaction could be initiated by a radical due to its reaction with an unsaturated fatty acid in the presence of oxygen, leading to the formation of a peroxy radical, which in turn can react with other nearby lipid molecules to generate additional lipid radicals. Besides, the cell debris was less dispersed in water than the soluble IOM fraction. Therefore, it is reasonable to infer that the cell debris would not compete as much ROS as IOM in the photocatalytic inactivation experiments and hence played a moderate role in decelerating the photocatalytic inactivation efficiency. With the addition of both IOM and cell debris, the “shoulder” extended to 2 h. In general, the extent of inhibition for photocatalytic inactivation followed: IOM + cell debris > IOM > cell debris. This trend highlighted that the IOM play a major role in the deceleration of photocatalytic bacterial inactivation process.

### 3.2. Evolution of the bulk parameters

To monitor the evolution of the released organic matters during the photocatalytic bacterial inactivation, the bulk parameters including protein, TOC and TN concentrations were measured along with time (Fig. 1b and c). As shown in Fig. 1b, trace amount of protein (~0.7 mg/L) were detected in the bulk solution at  $t = 0$  min, which was probably due to the release of soluble microbial product (SMP) from metabolic activity (Ni et al., 2011). The bulk protein concentration first dropped to 0.3 mg/L at  $t = 20$  min, and then soared up at  $t = 30$  min. It was worth noted that, from  $t = 0$  min to  $t = 30$  min (Stage I), approximately 3 log (99.9%) cells were inactivated (Fig. 1a). Considering the mechanism that the cell membrane is the primary target for the attack by ROS, the increased amount of protein in bulk was likely attributed to the leakage of intracellular protein through the damaged cell membrane, and the rate of leakage was faster than that of damage. From  $t = 30$  min to  $t = 2$  h (Stage II), the bulk protein concentration slightly increased to a maximum of 3.7 mg/L at  $t = 1$  h and then underwent a drastic drop. Taken the deterioration of bulk protein and deceleration of bacterial inactivation rate together at Stage II, we can conclude that the released protein could compete for the photo-generated ROS and subsequently lead to a deceleration of inactivation efficiency. After the cells were completely inactivated ( $t = 4$  h), we observed a fluctuated increasing trend of the bulk protein concentration. This increase can be ascribed to the ROSs continuously attack the inactivated cell skeleton thus rendered more protein being released into the bulk. A drop in protein concentration at  $t = 8$  h was possibly due to the released protein subsequently being adsorbed by the photocatalysts or photocatalytically degraded. Typically, the complete disruption of cell skeleton by photocatalysis required much longer time than completely inactivation as demonstrated by

the TEM and SEM images in our previous studies (Gao et al., 2012; Wang et al., 2012; Shi et al., 2014).

TOC and TN are important indexes of water quality. As seen in Fig. 1c, the bulk TOC and TN both increased and reached a maximum at  $t = 6$  h (16.8 mg C/L for TOC and 9.3 mg N/L for TN). It is worth noting that the maximum bulk TOC did not exceed either the TOC of IOM or that of cell debris (21.0 and 17.4 mg/L for IOM and cell debris, respectively, with an equivalent cell density of  $2 \times 10^8$  cfu/mL) as shown in Table 1, which indicated neither IOM nor cell debris were completely released into the bulk at  $t = 6$  h. Afterward, the TOC started to decrease gradually, whereas TN remained leveled off, suggesting that the bulk TOC could be further mineralized while the TN could not be removed by photocatalysis in the presence of dissolved oxygen. In principle, the photocatalytic oxidation end-products of carbon and nitrogen will be carbon dioxide ( $\text{CO}_2$ ) and nitrate ( $\text{NO}_3^-$ ), respectively. Since  $\text{CO}_2$  can volatilize into air whereas the  $\text{NO}_3^-$  will be retained in solution, the photocatalytic bacterial inactivation process will finally end up in nitrogen-rich solution as indicated by a consistent increasing TN/TOC ratio with increasing reaction time (Fig. 1c). It is of significance to note that nitrogen is an essential element for the growth of microorganisms, and is one of the major reasons to cause eutrophication (Conley et al., 2009). Therefore, post-treatment might be required to tackle the dissolved nitrogen to avoid potential risks such as growth of microorganism in pipeline or eutrophication in natural environment.

### 3.3. Changes in bulk solution absorption spectra of *E. coli* cells, IOM and cell debris by photocatalysis

The absorption spectra allow one to readily estimate the water quality such as aromaticity or the presence of nitrate/nitrite (Rieger et al., 2004; Matilainen et al., 2011). Fig. 2 shows the changes in bulk absorption spectra of *E. coli* cells, IOM and cell debris treated by photocatalysis along with irradiation time. As for the *E. coli* cells (Fig. 2a), generally, the intensities in the region of 200–250 nm, which was mainly responsible for the nitrate/nitrite (peak at 220 nm) (Rieger et al., 2004), increased along with increasing time, probably suggesting that the oxidation of organic nitrogen into nitrate/nitrite, which was then released into the bulk. For the untreated IOM (Fig. 2b), there was a peak at  $\sim 254$  nm, which was mainly due to  $\pi - \pi^*$  transitions of aromatic ring (Matilainen et al., 2011). This peak decayed substantially at the very beginning of the photocatalytic reaction, suggesting that the aromatic chromophores were preferentially oxidized by ROSS. This is in agreement with a previous report on the ability of photocatalysis to attack the aromatic ring of tryptophan by a mechanism of hydroxylation initiated by the photo-generated  $\cdot\text{OH}$  (Elsellami et al., 2010). In bacterial cells, the aromaticity mainly results from proteins that contain aromatic amino acids such as tryptophan, tyrosine and phenylalanine (Nelson and Cox, 2004). These amino acids are essential for lives and their high susceptibility may possibly play a role in the mechanism photocatalytic bacterial inactivation, besides

**Table 1**

The TOC concentration of the cell debris and bulk parameters and  $F_{\text{max}}$  of the four PARAFAC components of the IOM obtained from the fractionation procedure. The cell debris and IOM were in an equivalent cell density of  $2 \times 10^8$  cfu/mL.

Cell debris mg/L	IOM			PARAFAC components (Raman unit)			
	Bulk parameter (mg/L)			C1	C2	C3	C4
TOC	TOC	TN	Protein				
17.4	21.0	8.5	15.9	59.1	0	37.8	0.5

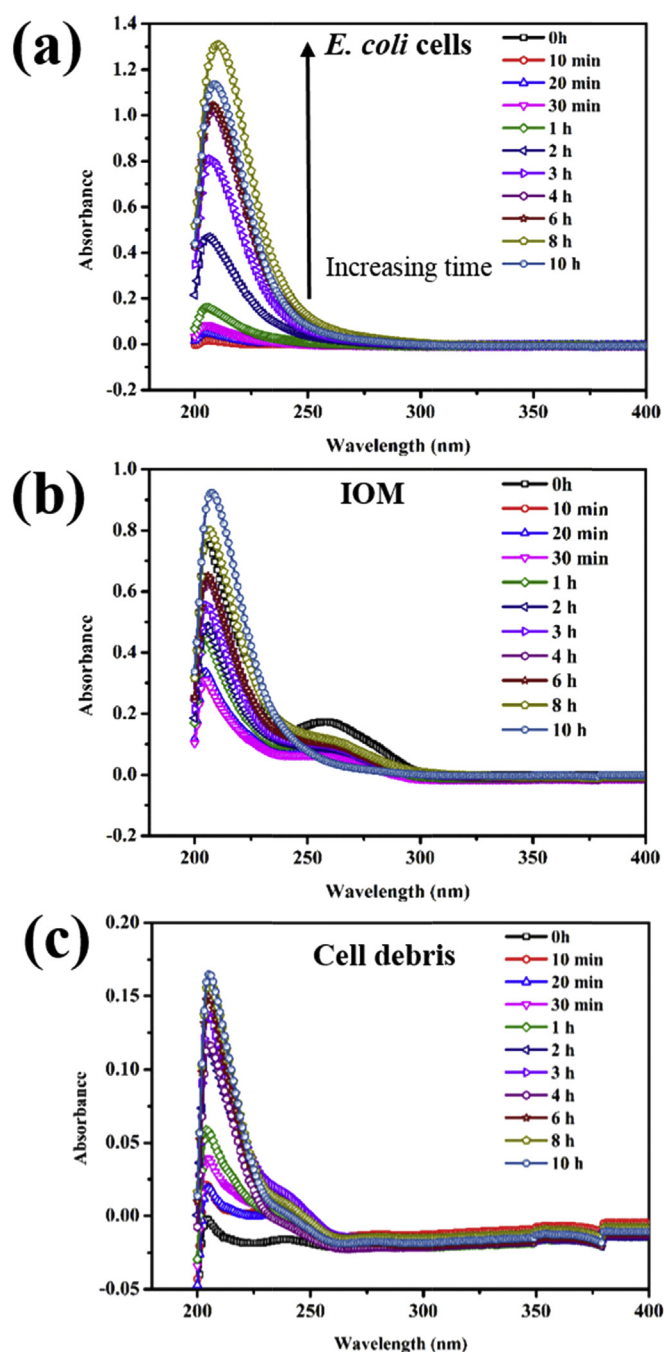


**Fig. 2.** Changes in the bulk absorption spectra of (a) *E. coli* cells, (b) IOM and (c) cell debris treated by  $\text{TiO}_2$ -UVA.

lipid peroxidation (Carre et al., 2014). The bulk absorbance of cell debris treated by  $\text{TiO}_2$ -UVA exhibited the same trend as the live *E. coli* cells but with a relatively low intensity, suggesting the bulk organic compounds might mainly originate from the IOM other than the cell debris. A shoulder peak at 225–250 nm appeared and increased in the bulk absorbance of cell debris along with reaction time, indicating the formation of peroxidized phospholipid (Kim and Labella, 1987; Souza et al., 2011) as a result of lipid peroxidation. This phenomenon was not observed in the *E. coli* cells samples which could be attributable to the high intensities of the broad major peak at 200–250 nm in the bulk of the *E. coli* samples. Additionally, we observed no absorbance for all the samples in the



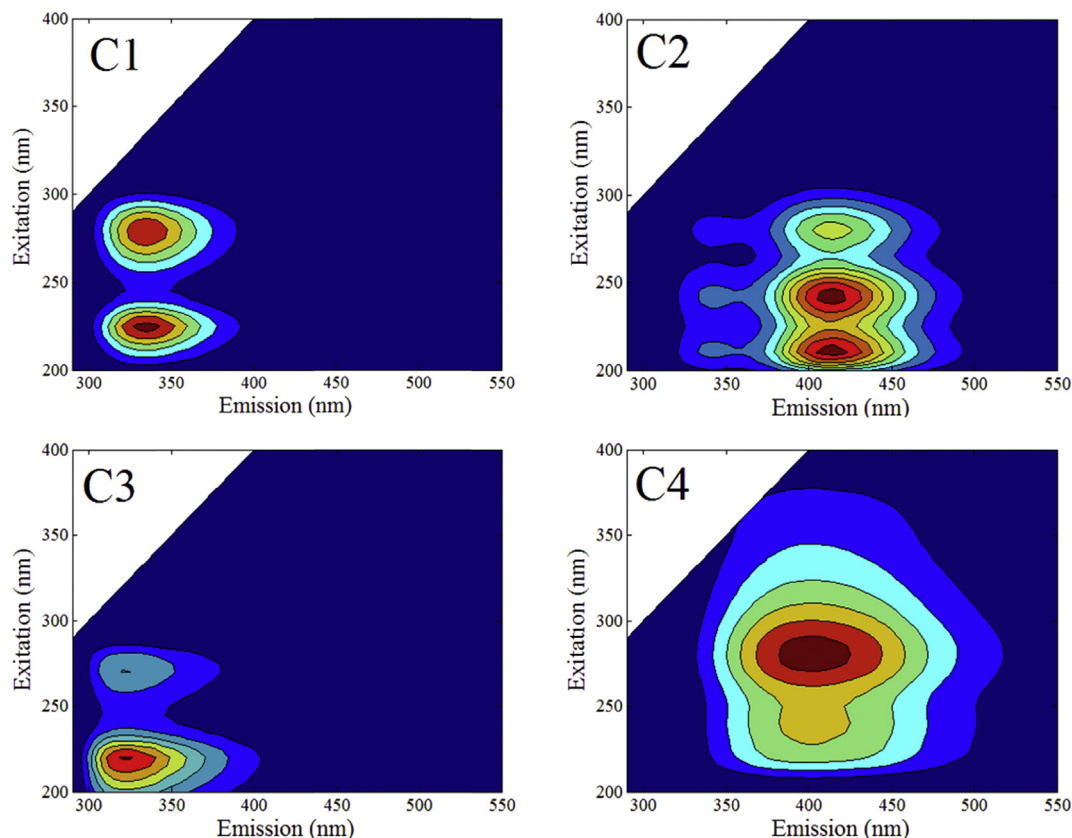


Fig. 4. EEM contours of the four components obtained by the PARAFAC analysis.

region of 300–400 nm, which covers the peak of UVA light source in this study (Fig. S2). Therefore, the possibility that the released organic matters would compete for photons with the photocatalysts and lead to deceleration of the inactivation rate is negligible.

### 3.4. Fluorescence EEM spectra

In this study, the fluorescence EEM spectra of the bulk samples of *E. coli* cells, IOM and cell debris treated by TiO<sub>2</sub>-UVA were obtained to get in-depth insight into the evolution of the released organic matters, and the EEM contours of the each treatment along with time are illustrated in Fig. 3. Before irradiation ( $t = 0$  h), two distinct peaks presented at Ex/Em of 280/330 and 220/330 nm were observed for all the three samples. According to the previous studies, these two peaks were associated with the protein-like substances (Hudson et al., 2007). Generally, changes in the fluorescence intensities and shape in the EEM contour plots were observed along with time for each photocatalytic experiments. Specifically, after 1 h of irradiation, new peaks located at Ex/Em of 280/430, 220/415 nm appeared, accompanied by the decay of the original peaks in the bulk *E. coli* cells. Similar trend was observed for the IOM, whereas there were three distinct new peaks located at Ex/Em of 285/405, 250/415 and 220/405 nm. As for the cell debris, three new peaks located at Ex/Em of 210/415, 240/415 and 280/415 nm appeared at the early stage of irradiation ( $t = 10$  min) and remained steady until the end of the experiment. These results suggested that the degradation of proteins and formation of fluorescence EEM byproducts occurred during the photocatalytic treatments, and different fractions had different potential in the formation of byproducts. Interestingly, intensities of new peaks in

the *E. coli* cells and IOM were both observed to decrease after 6 h, suggesting that the byproducts could be further degraded upon photocatalysis.

### 3.5. PARAFAC analysis

To get more detailed information of the fluorophores changes of the photocatalytic experiments, PARAFAC analysis was applied to decompose the fluorescence EEM data. Four components were identified and validated by residual analysis (Fig. S3) and half-split analysis (Fig. S4). As shown in Fig. 4, components 1 (C1) exhibited a two peaks Ex/Em of 225/335 and 280/335 nm, which was associated with tryptophan-like proteins (Hudson et al., 2007). Component 2 (C2) had three peaks located at Ex/Em of 210/415, 240/415 and 280/415 nm. Components 3 (C3) had characteristic peaks at Ex/Em of 270/320 and 220/320, which was attributed to tyrosine-like proteins (Hudson et al., 2007). Components 4 (C4) had a prominent peak Ex/Em at 280/405 nm. Tryptophan and tyrosine-like proteins (C1 and C3) are important constituents of microorganisms and they were commonly found in microbial systems using EEM-PARAFAC analysis (Ni et al., 2009; Xu et al., 2013). The detailed classification of C2 and C4 remained unknown and will be discussed in the following sections.

First of all, we noted that the  $F_{\max}$  of C1 and C3 in the IOM decreased remarkably (from 59.1 to 32.7 and from 37.8 to 2.9 R.U., respectively) after mixing with TiO<sub>2</sub> nanoparticles (Table 1 and Fig. 5), demonstrating that considerable amount of IOM protein had relatively high absorption ability on the TiO<sub>2</sub> nanoparticles, which is in agreement with our previous findings that protein are preferentially absorbed on the TiO<sub>2</sub> nanoparticles surfaces to form nanoparticle-protein 'corona'. Considering this phenomenon, we

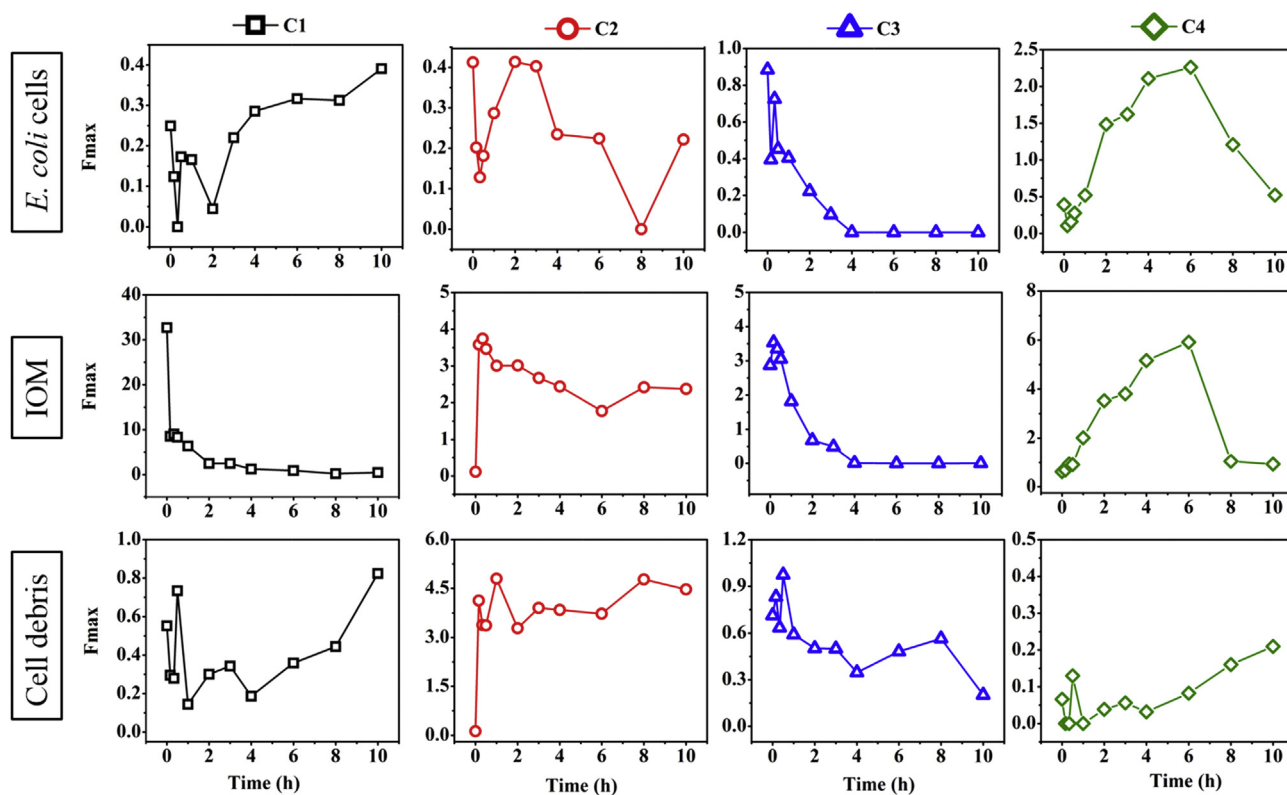


Fig. 5. Changes of maximum fluorescence intensity ( $F_{\max}$ ) for the four components of (a) *E. coli* cells, (b) IOM, and (c) cell debris treated by  $\text{TiO}_2$ -UVA.

could postulate that the deceleration of the inactivation of bacteria inactivation rate by released and spiked IOM (“tailing” and “shoulder”) in Fig. 1a could be attributed to two possibilities: (i) inhibit direct contact between nanoparticles and bacteria by absorbing on the  $\text{TiO}_2$  nanoparticles surface; (ii) compete for ROS with residual bacteria cell membrane.

The maximum fluorescence intensities ( $F_{\max}$ ) of the four components of each photocatalytic experiments as a function of time are shown in Fig. 5. It was found that the  $F_{\max}$  of C1 for *E. coli* cells and cell debris fluctuated and generally exhibited an increasing trend similar to that of protein evolution (Fig. 1b). This result implied that bulk C1 could be a rough indicator of protein that are being released into bulk, considering the fact that tryptophan is an important building block of protein. In contrast, C3 was found to decrease along with irradiation time for *E. coli* cells and cell debris, indicating a faster rate of degradation or adsorption than that of release for tyrosine-like protein. It was also found that  $F_{\max}$  of C2 and C4 in the fractions of IOM and cell debris were close to 0 R.U., indicating they were not original components of IOM or cell debris. Interestingly, we observed a significant increase in  $F_{\max}$  for C2 and C4 upon irradiation, followed by peak off with prolonged irradiation time. These results indicated that C2 and C4 mainly originated from the photocatalytic oxidation of the cellular components and they could be further degraded by photocatalysis. We also observed that C2 and C4 existed in the control experiments of *E. coli* cells (with  $\text{TiO}_2$  under dark, without  $\text{TiO}_2$  under light and without  $\text{TiO}_2$  under dark) initially (Fig. S5), and their intensities exhibited a slightly increasing trend but significantly lower than those of the photocatalytic treated IOM. The occurrence of C2 and C4 in the non-photocatalytic treated samples could be explained by the oxidative stress induced by environmental stress (i.e. the presence of nanoparticles, UVA irradiation or starvation) to the bacteria (Mandel and

Silhavy, 2005; Pigeot-Remy et al., 2012; Manke et al., 2013). In addition, C2 was found to initially present in the bulk of *E. coli* cells with a  $F_{\max}$  of ~0.4 R.U. and this background could be due to the oxidative stress induced by oxygen-respiring activity of the live bacteria (Imlay, 2013). However, the  $F_{\max}$  of C2 in the *E. coli* cells fluctuated along with photocatalytic reaction time and remained below the background value, suggesting that C2 was not a suitable parameter to indicate photocatalytic oxidation.

Indeed, for the photocatalytic treatment of *E. coli* cells and cell debris, the concentrations of each organic compound existed in the bulk solution is rather dynamic and could be determined by a combination effect of release, adsorption and degradation, and thus complicating the interpretation of the evolution of the PARAFAC EEM components along with irradiation time. Therefore, it is of particular interest to analyze the data obtained from IOM fractions because the releases of organic substances from insoluble fractions of cells were eliminated. The Person correlation analysis of the PARAFAC EEM components of IOM showed that C1 was negatively correlated with C2 ( $R = -0.557$ ,  $p < 0.05$ ) whereas C3 negatively correlated with C4 ( $R = -0.638$ ,  $p < 0.05$ ) (see Table 2). Considering the fact that fluorophores typically contain aromatic groups (Lakowicz, 2013) and that the negative correlation of C1 and C2, and that of C3 and C4, C2 and C4 were possibly originated from the photocatalytic modification byproducts of C1 and C3, respectively, that still maintained aromatic groups (fluorophores). A previous study on the degradation of pure tryptophan by  $\text{TiO}_2$ -UVA reported that there were formation of aromatic intermediates through (i) hydroxylation on the aromatic ring by  $\bullet\text{OH}$  considering an electrophilic attack; (ii) elimination of amino groups by  $e^-$ ; and (iii) removal of the carbon that bearing carboxylic acid and amino group by  $\bullet\text{OH}$  attack (Elsellami et al., 2010). Considering that change of substituents on the aromatic groups would lead to the change of

**Table 2**  
Pearson correlation between the  $F_{\max}$  of the four PARAFAC components for IOM treated by  $\text{TiO}_2$ -UVA.

	C1	C2	C3	C4
C1	1	-0.557 <sup>a</sup>	0.641 <sup>a</sup>	-0.460
C2		1	0.252	-0.130
C3			1	-0.638 <sup>a</sup>
C4				1

<sup>a</sup> Correlation is significant at the 0.05 level.

the fluorescence profile, therefore, the C2 and C4 were very likely the aromatic intermediates as a result of the photo-generated ROS attack on C1 and C3 in a mechanism. So far, the detailed structures of C2 and C4 remained unknown and merited further study in the future.

Cluster analysis of the dataset obtained from photocatalytic experiments of each fraction and bacteria (Fig. S6) indicates that the released organic substances during the photocatalytic inactivation of *E. coli* cells mainly derived from the photocatalytic degradation products of IOM other than the cell membranes. This is in good agreement with the PARAFAC analysis results, in which the C4 exhibits similar evolution profile and relatively high intensities in the bulk *E. coli* cells and IOM, while C4 in the bulk cell debris showed slightly increase along with irradiation time. Therefore, the domination of C4 might be used as an indicator of photocatalytic damage to cell membrane as well as the degradation of the released IOM.

### 3.6. Toxicity test

The toxicity of the treated water from photocatalytic inactivation of normal *E. coli* cells at different reaction time were assayed. Table 3 shows the EC50 results together with their respective toxicity units. No toxicity (EC50 > 99%) were detected at the beginning of the photocatalytic treatment (0–30 min). It is noteworthy that toxicity appeared after 1 h (EC50 = 91.3%) and increased until a maximum at  $t = 4$  h (EC50 = 55.74%), which corresponded to the time necessary to the complete inactivation of bacteria (Fig. 1a). Afterward, a decrease in toxicity was observed and finally complete detoxification was achieved. These results suggest that some toxic by-products were formed during the photocatalytic bacterial inactivation process, and these generated by-products could be further degraded/detoxified by this treatment.

To quantitatively investigate whether there is any relationship between the toxicity and four fluorescent components, we performed linear regression for the toxicity unit and  $F_{\max}$  using the linear fit equation:

**Table 3**  
Toxicity of various samples according to Microtox<sup>®</sup> test.

Time (h)	EC50 (%)	Toxicity unit	95% confidence interval	R <sup>2</sup>
0	>99	1.00	NA	NA
0.16	>99	1.00	NA	NA
0.33	>99	1.00	NA	NA
0.5	>99	1.00	NA	NA
1	91.3	1.10	84.59–98.53	0.988
2	70.75	1.41	67.46–74.2	0.995
3	71.88	1.39	67.46–76.58	0.987
4	55.74	1.79	51.32–60.55	0.982
6	63.02	1.59	54.93–72.3	0.918
8	>99	1.00	NA	NA
10	>99	1.00	NA	NA

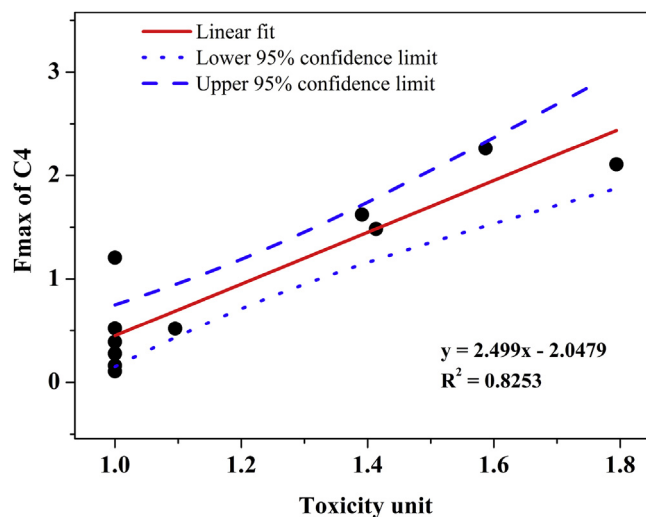


**Fig. 6.** Linear regression between the toxicity unit and maximum fluorescence intensity ( $F_{\max}$ ) of C4.

$$Y = A \times X + B \quad (3)$$

Where  $Y$  and  $X$  are the  $F_{\max}$  of the four fluorescent components and toxicity unit, respectively. Results indicate that only C4 exhibit a significant ( $R^2 = 0.8253$ ,  $p < 0.05$ ) linear correlation with the toxicity unit and is shown in Fig. 6. The fit parameters  $A$  and  $B$  were determined as 2.49904 and  $-2.04789$  with the intervals of [1.63216, 3.36592] and  $[-3.12142, -0.97437]$ , respectively, at a confidence level of 95%. Thus, it can be deduced that the maximum fluorescence intensity of C4 can be used as a quantitative indicator of toxicity.

During the past decades, the photocatalytic bacterial inactivation mechanism has attracted considerable research interests and different depths of knowledge have been obtained, however, little attention has been pay to the final product of photocatalytic disinfection, which purpose is to get clean and safe water. One major concern regarding the potential risks of photocatalytic disinfection technologies is to release toxic by-products. Results of this study demonstrated that toxicity occurred during the photocatalytic disinfection process, even at the time when the bacteria were completely inactivated. More crucially, the toxicity can be migrated if provided a longer reaction time. Of particular interest is the link between the toxicity and fluorescence component C4. As a result, monitoring the fluorescent components of water could be a valuable surrogate for photocatalytic bacterial inactivation or other hydroxyl radical ( $\bullet\text{OH}$ )-based disinfection technologies.

## 4. Conclusions

This study for the first time systematically investigates the organic matters released from the photocatalytic bacterial inactivation through fractionation procedure and spectroscopic analysis. The major conclusions can be drawn as follows:

- The released organic matters would be either absorbed on the surface of the photocatalysts or consume the photo-generated ROSs to decelerate the inactivation of the remaining cells as reflected by a plateau in the inactivation curve (“tailing”).
- EEM-PARAFAC analysis identified four fluorescence components during the photocatalytic inactivation of bacteria. Two

components (C1 and C3) were attributed to tryptophan and tyrosine-like proteins from the original cells, while the other two (C2 and C4) were postulated to be their oxidation by-products, respectively. More importantly, these by-products were subjected to photocatalytic degradation with prolonged reaction time.

- Toxicity occurred during the photocatalytic bacterial inactivation. Interestingly, we found that the toxicity shows a high linear relationship with the C4.
- The 3-D fluorescent fingerprint could be used as a surrogate to rapidly detect IOM release and their oxidation as well as toxicity in the photocatalytic bacterial inactivation.

## Acknowledgement

The project was supported by a research grant (GRF14100115) of the Research Grant Council, and a research grant (ITS/216/14) of Innovation Technology Support Program-Tier 3 Scheme of Innovation and Technology Commission Hong Kong SAR Government. The project was also supported by a Direct Grant from the Research Committee and a Technology and Business Development Fund (TBF15SCI008) from the Office of Research and Knowledge Transfer Services of The Chinese University of Hong Kong, and the research grant (41373102 and 21077104) of National Science Foundation of China to T.C. An and G.Y. Li. P.K. Wong was also supported by CAS/SAFEA International Partnership Program for Creative Research Teams.

## Appendix A. Supplementary data

Supplementary data related to this article can be found at <http://dx.doi.org/10.1016/j.watres.2016.12.032>.

## References

- Baghoth, S.A., Sharma, S.K., Amy, G.L., 2011. Tracking natural organic matter (NOM) in a drinking water treatment plant using fluorescence excitation-emission matrices and PARAFAC. *Water Res.* 45 (2), 797–809.
- Benabbou, A.K., Derriche, Z., Felix, C., Lejeune, P., Guillard, C., 2007. Photocatalytic inactivation of *Escherichia coli* - effect of concentration of TiO<sub>2</sub> and microorganism, nature, and intensity of UV irradiation. *Appl. Catal. B Environ.* 76 (3–4), 257–263.
- Carre, G., Hamon, E., Ennahar, S., Estner, M., Lett, M.C., Horvatovich, P., Gies, J.P., Keller, V., Keller, N., Andre, P., 2014. TiO<sub>2</sub> photocatalysis damages lipids and proteins in *Escherichia coli*. *Appl. Environ. Microbiol.* 80 (8), 2573–2581.
- Chong, M.N., Jin, B., Chow, C.W.K., Saint, C., 2010. Recent developments in photocatalytic water treatment technology: a review. *Water Res.* 44 (10), 2997–3027.
- Conley, D.J., Paerl, H.W., Howarth, R.W., Boesch, D.F., Seitzinger, S.P., Havens, K.E., Lancelot, C., Likens, G.E., 2009. Controlling eutrophication: nitrogen and phosphorus. *Science* 323 (5917), 1014–1015.
- Dalrymple, O.K., Stefanakos, E., Trotz, M.A., Goswami, D.Y., 2010. A review of the mechanisms and modeling of photocatalytic disinfection. *Appl. Catal. B Environ.* 98 (1–2), 27–38.
- Dietrich, A.M., Burlingame, G.A., 2015. Critical review and rethinking of USEPA secondary standards for maintaining organoleptic quality of drinking water. *Environ. Sci. Technol.* 49 (2), 708–720.
- Elsellami, L., Vocanson, F., Dapozze, F., Baudot, R., Febvay, G., Rey, M., Houas, A., Guillard, C., 2010. Kinetics and initial photocatalytic pathway of tryptophan, important constituent of microorganisms. *Appl. Catal. B Environ.* 94 (1–2), 192–199.
- Gao, M.H., An, T.C., Li, G.Y., Nie, X., Yip, H.Y., Zhao, H., Wong, P.K., 2012. Genetic studies of the role of fatty acid and coenzyme A in photocatalytic inactivation of *Escherichia coli*. *Water Res.* 46 (13), 3951–3957.
- Hu, J.Y., Ong, S.L., Shan, J.H., Kang, J.B., Ng, W.J., 2003. Treatability of organic fractions derived from secondary effluent by reverse osmosis membrane. *Water Res.* 37 (19), 4801–4809.
- Hudson, N., Baker, A., Reynolds, D., 2007. Fluorescence analysis of dissolved organic matter in natural, waste and polluted waters - a review. *River Res. Appl.* 23 (6), 631–649.
- Imlay, J.A., 2013. The molecular mechanisms and physiological consequences of oxidative stress: lessons from a model bacterium. *Nat. Rev. Microbiol.* 11 (7), 443–454.
- Ishii, S.K.L., Boyer, T.H., 2012. Behavior of reoccurring PARAFAC components in fluorescent dissolved organic matter in natural and engineered systems: a critical review. *Environ. Sci. Technol.* 46 (4), 2006–2017.
- Kim, R.S., Labella, F.S., 1987. Comparison of analytical methods for monitoring autoxidation profiles of authentic lipids. *J. Lipid Res.* 28 (9), 1110–1117.
- Korak, J.A., Wert, E.C., Rosario-Ortiz, F.L., 2015. Evaluating fluorescence spectroscopy as a tool to characterize cyanobacteria intracellular organic matter upon simulated release and oxidation in natural water. *Water Res.* 68, 432–443.
- Lakowicz, J.R., 2013. Principles of fluorescence spectroscopy. Springer Science & Business Media.
- Lambert, R.J.W., Johnston, M.D., 2001. The effect of interfering substances on the disinfection process: a mathematical model. *J. Appl. Microbiol.* 91 (3), 548–555.
- Lawaetz, A.J., Stedmon, C.A., 2009. Fluorescence intensity calibration using the raman scatter peak of water. *Appl. Spectrosc.* 63 (8), 936–940.
- Leung, T.Y., Chan, C.Y., Hu, C., Yu, J.C., Wong, P.K., 2008. Photocatalytic disinfection of marine bacteria using fluorescent light. *Water Res.* 42 (19), 4827–4837.
- Li, L., Wang, Z.M., Rietveld, L.C., Gao, N.Y., Hu, J.Y., Yin, D.Q., Yu, S.L., 2014. Comparison of the effects of extracellular and intracellular organic matter extracted from *Microcystis aeruginosa* on ultrafiltration membrane fouling: dynamics and mechanisms. *Environ. Sci. Technol.* 48 (24), 14549–14557.
- Mandel, M.J., Silhavy, T.J., 2005. Starvation for different nutrients in *Escherichia coli* results in differential modulation of RpoS levels and stability. *J. Bacteriol.* 187 (2), 434–442.
- Maness, P.C., Smolinski, S., Blake, D.M., Huang, Z., Wolfrum, E.J., Jacoby, W.A., 1999. Bactericidal activity of photocatalytic TiO<sub>2</sub> reaction: Toward an understanding of its killing mechanism. *Appl. Environ. Microbiol.* 65 (9), 4094–4098.
- Manke, A., Wang, L.Y., Rojanasakul, Y., 2013. Mechanisms of nanoparticle-induced oxidative stress and toxicity. *Biomed. Res. Int.* <http://dx.doi.org/10.1155/2013/942916>.
- Marugan, J., van Grieken, R., Pablos, C., Sordo, C., 2010. Analogies and differences between photocatalytic oxidation of chemicals and photocatalytic inactivation of microorganisms. *Water Res.* 44 (3), 789–796.
- Marugan, J., van Grieken, R., Sordo, C., Cruz, C., 2008. Kinetics of the photocatalytic disinfection of *Escherichia coli* suspensions. *Appl. Catal. B Environ.* 82 (1–2), 27–36.
- Matilainen, A., Gjessing, E.T., Lahtinen, T., Hed, L., Bhatnagar, A., Sillanpaa, M., 2011. An overview of the methods used in the characterisation of natural organic matter (NOM) in relation to drinking water treatment. *Chemosphere* 83 (11), 1431–1442.
- Meng, F.G., Huang, G.C., Yang, X., Li, Z.Q., Li, J., Cao, J., Wang, Z.G., Sun, L., 2013. Identifying the sources and fate of anthropogenically impacted dissolved organic matter (DOM) in urbanized rivers. *Water Res.* 47 (14), 5027–5039.
- Nelson, D.L., Cox, M.M., 2004. Lehninger Principles of Biochemistry, fourth ed. W. H. Freeman, New York.
- Ni, B.J., Fang, F., Xie, W.M., Sun, M., Sheng, G.P., Li, W.H., Yu, H.Q., 2009. Characterization of extracellular polymeric substances produced by mixed microorganisms in activated sludge with gel-permeating chromatography, excitation-emission matrix fluorescence spectroscopy measurement and kinetic modeling. *Water Res.* 43 (5), 1350–1358.
- Ni, B.J., Rittmann, B.E., Yu, H.Q., 2011. Soluble microbial products and their implications in mixed culture biotechnology. *Trends Biotechnol.* 29 (9), 454–463.
- Pigeot-Remy, S., Simonet, F., Atlan, D., Lazzaroni, J.C., Guillard, C., 2012. Bactericidal efficiency and mode of action: a comparative study of photochemistry and photocatalysis. *Water Res.* 46 (10), 3208–3218.
- Pigeot-Remy, S., Simonet, F., Errazuriz-Cerda, E., Lazzaroni, J.C., Atlan, D., Guillard, C., 2011. Photocatalysis and disinfection of water: identification of potential bacterial targets. *Appl. Catal. B Environ.* 104 (3–4), 390–398.
- Rieger, L., Langergraber, G., Thomann, M., Fleischmann, N., Siegrist, H., 2004. Spectral in-situ analysis of NO<sub>2</sub>, NO<sub>3</sub>, COD, DOC and TSS in the effluent of a WWTP. *Water Sci. Technol.* 50 (11), 143–152.
- Shannon, M.A., Bohn, P.W., Elimelech, M., Georgiadis, J.G., Marinas, B.J., Mayes, A.M., 2008. Science and technology for water purification in the coming decades. *Nature* 452 (7185), 301–310.
- Shi, H.X., Li, G.Y., Sun, H.W., An, T.C., Zhao, H.J., Wong, P.K., 2014. Visible-light-driven photocatalytic inactivation of *E. coli* by Ag/AgX-CNTs (X = Cl, Br, I) plasmonic photocatalysts: bacterial performance and deactivation mechanism. *Appl. Catal. B Environ.* 158, 301–307.
- Souza, F.H., de Almeida, L.R., Batista, F.S.C., Rios, M.A.d.S., 2011. UV-visible spectroscopy study of oxidative degradation of sunflower biodiesel. *Energy Sci. Technol.* 2 (2), 56–61.
- Stedmon, C.A., Bro, R., 2008. Characterizing dissolved organic matter fluorescence with parallel factor analysis: a tutorial. *Limnol. Oceanogr.* 6, 572–579.
- Thabet, S., Simonet, F., Lemaire, M., Guillard, C., Cotton, P., 2014. Impact of photocatalysis on fungal cells: depiction of cellular and molecular effects on *Saccharomyces cerevisiae*. *Appl. Environ. Microbiol.* 80 (24), 7527–7535.
- Valencia, S., Marin, J.M., Restrepo, G., Frimmel, F.H., 2014. Evaluation of natural organic matter changes from Lake Hohloh by three-dimensional excitation-emission matrix fluorescence spectroscopy during TiO<sub>2</sub>/UV process. *Water Res.* 51, 124–133.
- Wang, Q., Yee, L.F., Hu, J.Y., 2014. Relationship between organic precursors and N-nitrosodimethylamine (NDMA) formation in tropical water sources. *J. Water Health* 12 (4), 736–746.
- Wang, W.J., Yu, Y., An, T.C., Li, G.Y., Yip, H.Y., Yu, J.C., Wong, P.K., 2012. Visible-light-driven photocatalytic inactivation of *E. coli* K-12 by bismuth vanadate nanotubes: bactericidal performance and mechanism. *Environ. Sci. Technol.* 46 (8), 4599–4606.
- Xu, H.C., Cai, H.Y., Yu, G.H., Jiang, H.L., 2013. Insights into extracellular polymeric

- substances of cyanobacterium *Microcystis aeruginosa* using fractionation procedure and parallel factor analysis. *Water Res.* 47 (6), 2005–2014.
- Yang, X.F., Meng, F.G., Huang, G.C., Sun, L., Lin, Z., 2014. Sunlight-induced changes in chromophores and fluorophores of wastewater-derived organic matter in receiving waters - The role of salinity. *Water Res.* 62, 281–292.
- Zor, T., Selinger, Z., 1996. Linearization of the Bradford protein assay increases its sensitivity: theoretical and experimental studies. *Anal. Biochem.* 236 (2), 302–308.